Investigations on alunogen under Mars-relevant temperature conditions: an example for a single-crystal-to-single-crystal phase transition

Volker Kahlenberg[1], Doris E. Braun[2] and Maria Orlova[1]

[1]Institute of Mineralogy and Petrography, University of Innsbruck, Innrain 52, A-6020 Innsbruck, Austria

[2]Institute of Pharmacy, Pharmaceutical Technology, Innrain 52c, A-6020 Innsbruck, Austria

*Mailing Address:

Volker Kahlenberg (corresponding author)

Institut für Mineralogie und Petrographie

Leopold-Franzens-Universität Innsbruck

Innrain 52

A- 6020 Innsbruck

e-Mail: Volker.Kahlenberg@uibk.ac.at phone: +43 (0)512 507 5503

e-Mail: Maria.Orlova@uibk.ac.at phone: +43 (0)512 507 5505

eMail: Doris.Braun@uibk.ac.at phone: +53 (0512) 507 58653

Running title: On the monoclinic low-temperature polymorph of alunogen.

Abstract

The low-temperature (LT) dependent behavior of a synthetic alunogen sample with composition $Al_2(SO_4)_3 \cdot 16.61H_2O$ has been studied in the overall temperature range from -100 to 23 °C by DSC measurements, *in-situ* powder and single-crystal X-ray diffraction as well as Raman spectroscopy. Cooling/heating experiments using the different techniques prove that alunogen undergoes a reversible, sluggish phase transition somewhere between -30 and -50 °C from the triclinic room-temperature (RT) form to a previously unknown LT-polymorph. A significant hysteresis for the transition was observed with all three methods and the transition temperatures were found to depend on the employed cooling/heating rates. The crystal structure of the LT-modification has been studied at -100 °C using single crystals which have been grown from an aqueous solution. Basic crystallographic data are as follows: monoclinic symmetry, space group type $P2_1$, a = 7.4125(3) Å, b = 26.8337(16) Å, c = 6.0775(3) Å, β = 97.312(4)°, V = 1199.01(10) Å^3 and Z = 2. Structure analysis revealed that LT-alunogen corresponds to a non-stoichiometric hydrate with 16.61 water moieties p.f.u. Notably, the first-order transition results in a single-crystal-to-single-crystal transformation. In the asymmetric unit there are two Al-atoms, three [SO_4]-tetrahedra, and seventeen crystallographically independent sites for water molecules, whose hydrogen positions could be all located by difference-Fourier calculations. According to site-population refinements only one water position (Ow5) shows a partial occupancy. A comfortable way to rationalize the crystal structure of the LT-modification of alunogen is based on a subdivision of the whole structure into two different slabs parallel to (010). The first type of slab (type A) is about nine Å thick and located at $y \approx 0$ and $y \approx ½$, respectively. It contains the $Al(H_2O)_6$-octahedra as well as the sulfate groups centered by S1 and S2. Type B at $y \approx ¼$ and $y \approx ¾$ comprises the remaining tetrahedra about S3 and a total of five additional "zeolitic" water sites (Ow1-Ow5) which are not a part of a coordination polyhedron. Within slab-type A alternating chains of (unconnected) octahedra and tetrahedra can be identified which are

48 running parallel to [100]. In addition to electrostatic interactions between the $Al(H_2O)_6^{3+}$- and
49 the $(SO_4)^{2-}$-units, hydrogen bonds are also essential for the stability of these slabs. A detailed
50 comparison between both modifications including a derivation from a hypothetical aristotype
51 based on group-theoretical concepts is presented. Since alunogen has been postulated to occur
52 in martian soils the new findings may help in the identification of the LT-form by X-ray
53 diffraction using the Curiosity Rover's ChemMin instrument or by Raman spectroscopy.
54
55
56 **Keywords**: alunogen, low-temperature phase transition, polymorphism, crystal-structure
57 determination, DSC-measurements, X-ray diffraction, Raman spectroscopy, multivariate data
58 analysis, group theory

Introduction

Most of the naturally occurring hydrous aluminum sulfates are basic hydrates containing water molecules and hydroxyl groups. Examples include the minerals aluminite ($Al_2(SO_4)(OH)_4 \cdot 7H_2O$), meta-aluminite ($Al_2(SO_4)(OH)_4 \cdot 5H_2O$), jurbanite ($Al(SO_4)(OH) \cdot 5H_2O$) and rostite ($Al(SO_4)(OH) \cdot 3H_2O$), just to mention a few. One of the rare OH-free compounds is alunogen. Usually, alunogen is chemically described as a heptadecahydrate corresponding to the formula $Al_2(SO_4)_3 \cdot 17H_2O$. Notably, the exact water content of alunogen has been a matter of debate for quite a long time and various compositions between sixteen and eighteen water molecules per formula unit (p.f.u.) have been reported (Larsen and Steiger 1928; Palache et al. 1951; Bayliss 1964; Barret and Thiard 1965; Náray-Szabó 1969; Menchetti and Sabelli 1974; Fang and Robinson 1976; Chou and Soong 1984; Çilgi and Cetişli 2009; Bai et al. 2011; Wang and Zhou 2014). This variability is a direct consequence of the fact that alunogen crystals which are exposed to air of low relative humidity at room temperature easily start to dehydrate partially, i.e. alunogen can be considered a non-stoichiometric hydrate (Fang and Robinson 1976). In addition to uncertainties concerning the precise amount of water present in alunogen using starting materials from different sources, there are also discrepancies between the results of thermoanalytical studies originating from different groups. Actually, the release of structural water in the range between ambient temperature and about 450°C has been reported to be connected with either two (Bayliss 1964; Földvári 2011) or four (Chou and Soong 1984; Çilgi and Cetişli 2009) step processes, respectively.

Natural alunogen occurs globally and about 250 different localities have been listed in the mindat.org database (http://www.mindat.org, accessed March 3rd, 2015). The mineral can be found in quite a number of different geological settings. The most important ones are associated with the oxidation of metal-sulfide mineral deposits or tailings impoundments in aride climates (Jambor et al. 2000 and references cited therein). Furthermore, alunogen has

been observed in alteration products of kaolinite by acid sulfate fluids in ignimbrite country rocks (Te Kopia geothermal field, New Zealand, Martin et al. 1999) or incrustations from exhalation-condensation processes related to fumarolic activities (Soufrière Hills Volcano, Caribbean island of Montserrat, Boudon et al. 1996). Another environment where alunogen comes into play is coal mining. The mineral has been discovered in larger quantities in burning coal mining waste dumps (Upper Silesian Coal basin, Poland, Kruszewski 2013) or as deposits derived from gases exhaled from surface vents associated with underground coal fires (Wuda coal field, Inner Mongolia, Stracher et al. 2005). Finally, its occurrence has been also reported from caves where it originated from reactions triggered by release of H_2S from sulfidic springs (Serpent cave, France, Audra and Hobléa 2007).

Moreover, hydrous sulfates also play an important role in the mineralogy of Mars. Orbital remote sensing in combination with data obtained from landed missions (Opportunity and Curiosity rovers, for example) have shown that various Ca-, Mg-, Fe-, and Al-sulfates are among the major secondary minerals on the surface of the "red planet" (Bibring et al. 2006; Swayze et al. 2008; Kounaves et al. 2010, Bish et al. 2013 and references cited therein). Only very recently, the dehydration behavior and rates of several sulfates including alunogen have been studied under Mars relevant pressure and partial water pressure conditions (Wang and Zhou 2014). Notably, low-temperature single-crystal diffraction data sets have been lacking for sulfate minerals for quite a long time (Mills et al. 2013). Furthermore, Al-sulfates have been found in alteration experiments on a basaltic tephra from Mauna Kea, Hawaii, that had a composition similar to the average Mars basaltic soil (Bell 2014) and on basaltic glasses (Golden et al. 2005, Hausrath et al. 2013).

So far, no detailed structural characterization of alunogen has been performed at low temperatures. However, these kinds of studies would be necessary to proxy for martian conditions since the global mean surface temperature on Mars is ~ -71 °C (Haberle 2013),

while local temperatures may lie within the range of at least -130 – 0 °C (Herri and Chassefière 2012).

Therefore, we decided to study the low-temperature behavior of alunogen using thermal, spectroscopic and diffraction techniques. Our investigations show that alunogen undergoes a reversible sluggish structural phase transition upon cooling. The new data may help in the identification of this mineral by X-ray diffraction of martian soils using the Curiosity Rover's ChemMin instrument (Bish et al. 2014) or by Raman spectroscopy.

Experimental details

For the DSC, the X-ray powder diffraction and Raman experiments a commercial sample of alunogen was used (VWR International, ACS grade) which was further carefully milled with an agate mortar and a pestle and stored for one month in a desiccator at 43% relative humidity fixed by a K_2CO_3-saturated solution. Determination of the absolute water content was performed using a Karl Fischer coulometric titrator C20 instrument (Mettler Toledo, Switzerland). The average value for a total of five measurements was 16.3 ± 0.3 mole water per mole $Al_2(SO_4)_3$.

Differential scanning calorimetry was conducted using a DSC 204 F1 Phoenix (Netzsch-Gerätebau GmbH, Selb, Germany) equipped with a liquid nitrogen cooling device and operated with the Proteus software package version 4.8.5. Approximately 27 milligrams of sample were weighed (Mettler UM3 ultramicrobalance) into sealed Al-pans. Dry nitrogen was used as purge gas (purge: 20 ml min^{-1}) and liquid nitrogen for the cooling process. The measurements were recorded with a heating/cooling rate of 10 °C min^{-1} in the temperature range between –80 and 40 °C. The instrument was calibrated for temperature with Hg (m.p. –38.8 °C), benzophenone (48.0 °C), In (156.6 °C), Sn (231.9 °C), Bi (271.4 °C) and Zn (419.6 °C), and the energy calibration was performed with Hg (heat of fusion 11.4 J g^{-1}), In (28.6 J g^{-1}), Sn (60.5 J g^{-1}), Bi (53.1 J g^{-1}) and Zn (60.5 J g^{-1}). The error on the extrapolated transition enthalpy, 95% confidence interval (CI), was derived from three measurements.

A first inspection of the commercial sample before milling under a petrographic microscope revealed that the material consisted of platy single crystals up to 50 μm in size. Due to an extensive intergrowth of the crystals, however, it was not possible to retrieve a sample of sufficient size for single-crystal structure analysis by simply separating the aggregates using a scalpel blade. Consequently, we finally decided to grow larger single crystals from an aqueous solution by slow evaporation of the solvent. Therefore, 1 g of the commercial material was dissolved in 65 ml of distilled water contained in a 250 ml glass beaker. The open beaker was stored at 23(2) °C and 43% relative humidity. Solidification started after about four days from the upper surface of the solution by the formation of a gel-like crust which completely covered the liquid phase within one week. After four weeks, an inspection of the volume below the crust revealed the presence of well-separated, optically transparent, birefringent crystals with an extremely thin-plate morphology (dimensions: 500 x 500 x 5 μm^3) in contact with solution.

About twenty of the crystals retrieved from the liquid were screened under a polarizing binocular. In all cases no clear extinction position could be found when observed with crossed Nicols, thus indicating twinning of at least two domains with different orientations of the indicatrix. Notably, this type of twinning has been already reported by Menchetti and Sabelli (1974) as a characteristic feature of triclinic alunogen. Unfortunately, the twin plane is parallel to the basal planes of the thin plates, making it impossible to separate the individuals mechanically. Therefore, we finally decided to perform the structural investigations with a larger twinned specimen. The crystal was mounted on the tip of a glass fiber with finger-nail hardener. Single-crystal diffraction studies have been performed on an Oxford Diffraction Gemini Ultra diffractometer using ω-scans. Preliminary diffraction experiments using graphite-monochromatized Mo-*K*α radiation showed the expected complex diffraction pattern resulting from the superposition of the reciprocal lattices of two triclinic individuals.

Nevertheless, diffraction spots coming from the different domains could be indexed independently. Unit-cell parameters at ambient temperature were as follows: a = 7.4133(5) Å, b = 26.910(2) Å, c = 6.0466(3) Å, α = 90.036(6)°, β = 97.612(5)° and γ = 91.868(6)°. They are in good agreement with literature data for triclinic alunogen (Menchetti and Sabelli 1974; Fang and Robinson 1976).

For the low-temperature studies the sample was flash-cooled to -100(2) °C in a dried compressed air stream produced from an Oxford Cryosystems Desktop Cooler unit. Preliminary investigations showed that under these conditions (i) splitting of the reflections due to twinning had disappeared and (ii) the frames could be indexed with a primitive-monoclinic unit cell, closely related to the triclinic room-temperature (RT) metric. Both observations pointed to the existence of a structural phase transition upon cooling the sample from ambient conditions to the target temperature. Regular determinations of the unit-cell volume at -100(2) °C over a period of eight hours did not show any systematic decrease of this parameter which should be expected for a release of water in the cold dry gas stream. In order to characterize the low-temperature (LT) modification in more detail, a data set corresponding to a hemisphere of reciprocal space was collected at -100(2) °C. Subsequent integration and data reduction including Lorentz and polarization corrections was performed with the *CrysAlis PRO* software package (Agilent 2012). Furthermore, the data were analytically corrected for absorption using accurately measured crystal faces based on the procedure of Clark and Reid (1995). No extinction correction was applied. The observed Laue symmetry and extinction symbol 2/*m* *P*-2$_1$- resulted in the following possible space group types: *P*2$_1$ or *P*2$_1$/*m*. Structure determination was performed using direct methods (program SIR2004, Burla et al. 2005). Both space group types were tested. However, a crystallochemically reasonable model could be only obtained for the non-centrosymmetric symmetry (*P*2$_1$). This preliminary structure included the positions of the Al-, S- and the O-atoms and was subsequently refined by full-matrix least-squares methods based on F^2

(program SHELXL97, Sheldrick 2008). Neutral-atom scattering coefficients and anomalous dispersion corrections were taken from the *International Tables for Crystallography, Volume C* (Prince 2004). Difference-Fourier calculations were employed to reveal the positions of the missing hydrogen atoms. This procedure allowed the location of the hydrogens of all seventeen water sites in the asymmetric unit. The positional parameters of the H-atoms were further optimized by a riding model with water-molecule geometries restrained by DFIX 0.86 0.01 commands for the O-H and DFIX 1.35(2) commands for the H…H distances (giving H-O-H angles close to 105°). All non-hydrogen atoms were refined using anisotropic displacement factors. The displacement parameters for the H atoms of the water molecules were coupled to those of the corresponding oxygen atoms according to $U_{iso}(H) = 1.2 \times U_{eq}(O)$. Analysis of the Bijvoet differences using the Flack parameter (Flack 1983) pointed to the presence of racemic twinning. Introduction of the corresponding twin law into the refinement led to a ratio of 0.39(2):0.61(2) for the two racemic components. Final calculations resulted in a residual of R(|*F*|)= 0.0377. The largest shift/esd in the last cycle was < 0.001. An inspection of the fractional atomic coordinates using the ADDSYM algorithm implemented in the program PLATON (Spek 2009) did not reveal any indication for an unneccessarily low space-group symmetry. A summary of all relevant parameters related to data collection and structure refinement can be found in Table 1. Relative atomic coordinates and selected interatomic distances and angles are given in Tables 2 and 3. Additional tables containing the anisotropic displacement parameters as well as the hydrogen-bond geometries have been deposited. Drawings of structural details were prepared using the program ATOMS6.4 (Dowty 2011), ORTEP for Windows (Farrugia 2012) and VESTA 3 (Momma and Izumi 2011). A CIF-file containing all structural information has been deposited as supplementary material.

X-ray powder diffraction data were collected on a Stoe STADI MP diffractometer in transmission geometry using strictly monochromatic Cu-$K\alpha_1$ radiation from a focusing Ge(111) primary beam monochromator and a Mythen1k detector with 11° detection range.

The sample was contained in a 0.3 mm diameter borosilicate glass capillary which was spinned during data collection. Temperature-dependent measurements in the range between -100 to 20 °C in steps of ΔT = 10 °C have been made using an Oxford Cryosystems Desktop Cooler device. Data in the range from 19.2 to 20.85° 2θ with the 0.009° step size were collected in order to follow the phase transition (counting time per step: 360 sec; ramp rate between set points: 1 °C/sec; dwell time at the set points before starting the measurement: 10 min; total data collection time per scan: 2.5 h). Longer data collections have been performed at -100, -40, 20°C in the 2θ-range from 5 to 80°. The crystal structure of the LT-modification of alunogen was refined using the data set acquired at -100 °C and the model retrieved from the single-crystal structure determination in space group $P2_1$ by the Rietveld method with the TOPAS software package (Coelho 2007). The background was modelled by Chebychev polynomials up to 10^{th} order. Common isotropic displacement factors were used for each type of atoms except hydrogen. The refinement converged at R_B = 0.0528, R_p = 0.0544, R_{exp} = 0.0586, R_{wp} = 0.0717, χ^2 = 1.22. Final unit-cell parameters values were a = 6.0583(8)Å, b = 26.839(1) Å, c = 7.390(1)Å, β = 97.471(1)° and V = 1191.8(3) Å^3. The results of the structural refinements of the powder diffraction data were consistent with the single-crystal structure analysis (see Figure 1). For a better comparison between the powder diffraction patterns of both polymorphs the result of a LeBail-fit of the pattern collected for the triclinic form at 20 °C has been deposited as well. A table summarizing the observed d-values and relative intensities for the LT-form in the 2θ-region up to 40° can be found in the supplementary data.

Raman spectra were recorded with a Bruker RFS 100 Raman-spectrometer (Bruker Analytische Messtechnik GmbH, Germany), equipped with a Nd:YAG Laser (1064 nm) as the excitation source and a liquid-nitrogen-cooled, high-sensitivity Ge-detector. The spectra (256 scans per spectrum) were measured in aluminum sample holders with a laser power of 400 mW and a resolution of 4 cm^{-1}. Temperature conditions were adjusted with a SPECAC

(Grasebury Specac Limited, Orpington, UK) variable temperature cell and a temperature control unit. The cell was evacuated (200 mbar). Principal component analysis (PCA) was used to interpret the changes in Raman spectra during temperature cycling. Data were processed using the Simca-P software (Umetrics 2005). The spectral region from 1200 to 95 cm^{-1} was used for constructing the PCA models. Cross validation (leave-one-out) was used to validate the PCA models. The number of principal components (PCs) used in the PCA models were selected by the PRESS function (predicted residual error sum-of-squares).

Crystal structure of the LT-polymorph

Structure analysis showed that the crystal of the monoclinic low-temperature modification of alunogen corresponds to a non-stoichiometric hydrate with 16.61 water moieties p.f.u. In the asymmetric unit of the LT-form there are two Al-atoms, three [SO_4]-tetrahedra, and seventeen crystallographically independent sites for water molecules. Sixteen of those are fully occupied. According to site-population refinements only the water position Ow5 shows a partial occupancy of 61(1)%. This finding is in good agreement with the results of Menchetti and Sabelli (1974) as well as Fang and Robinson (1976) on the triclinic RT-form. Both groups reported water contents between sixteen and seventeen molecules in air of normal relative humidity for natural alunogen crystals.

The values for the S–O distances are in the normal range for sulfates (Hawthorne et al. 2000). The bonding situation in all SO_4-tetrahedra is rather balanced, i.e. the scatter in the distances and angles is not very pronounced. This is also reflected in the values for the quadratic elongation and the angle variance σ^2 (Robinson et al. 1971) that can be used for the numerical quantification of the distortion (see Table 3). Each aluminum cation in turn is coordinated by six water moieties in form of an octahedron (see Figure 2). Al–O distances vary between 1.855–1.897 Å (for Al1) and 1.849–1.877 Å (for Al2).

A comfortable way to rationalize the crystal structure of the LT-modification of alunogen is based on a subdivision of the whole structure into two different slabs parallel to (010). The first type of slab (type A) is about nine Å thick and located at $y \approx 0$ and $y \approx ½$, respectively. It contains the $Al(H_2O)_6$ - octahedra as well as the sulfate groups centered by S1 and S2. Type B at $y \approx ¼$ and $y \approx ¾$ comprises the remaining tetrahedra about S3 as well as a total of five additional "free" water sites (Ow1–Ow5) which are not a part of a coordination polyhedron. Within slab-type A alternating chains of (unconnected) octahedra and tetrahedra can be identified which are running parallel to [100] (Figure 3). In addition to electrostatic interactions between the $Al(H_2O)_6^{3+}$- and the $(SO_4)^{2-}$-units in these slabs also hydrogen bonds are essential for the stability of the structural fragments. A detailed summary of the total hydrogen bonding scheme of the H-atoms belonging to the twelve water molecules (O13–O24) of the coordination sphere of the aluminum ions can be found in the supplements. For both crystallographically independent octahedra the same principal arrangements can be observed. Each three water ligands (O13, O16, O17 and O20, O21, O22, respectively) are exclusively involved in hydrogen bonds with neighboring oxygens of the sulfate groups from the same slab-type. The H-atoms of two molecules (O14 and O24, respectively) have acceptors corresponding to oxygens of one $[SO_4]$-group from slab-type A as well as one from the "interspace" (slab-type B). Hydrogen bonds of the molecules O15, O18 and O19, O23, respectively, in turn have one water molecule from the interlayer as a potential acceptor.

The water molecules in slab-type B are hydrogen-bonded (i) to oxygens from different sulfate groups (Ow1, Ow2), (ii) to other water molecules from the slab (Ow3) or (iii) a combination of (i) and (ii) (Ow4, Ow5). A view of a single type B slab perpendicular to (010) with indicated hydrogen bonds is given in Figure 4.

Bond-valence sum (BVS) calculations for the atoms were based on the parameter sets given by Brown and Altermatt (1985) (for the Al–O and S–O bonds) as well as Brese and O'Keeffe

(1991) (for the O–H pair). The results in valence units (*v.u.*) including donor and acceptor contributions for the oxygen atoms involved in hydrogen bonds are listed in Table 2.

The crystal structure of the LT-polymorph of alunogen is almost isotypic to its selenate analogue whose composition has been reported to be $Al_2(SeO_4)_3 \cdot 16(H_2O)$ (Krivovichev 2006). For the calculation of several quantitative descriptors for the characterization of the degree of similarity between the LT-form of the sulfate and the selenate whose crystal structure has been determined at ambient temperatures, the program COMPSTRU (Tasci et al. 2012) was used. For the two compounds, the degree of lattice distortion (S), i.e. the spontaneous strain obtained from the eigenvalues of the finite Lagrangian strain tensor calculated in a Cartesian reference system, has a value of (S) = 0.0107. After a transformation according to **a**' = **c**, **b**' = **-b** and **c**' = **-a** plus an origin shift of (½, -0.0406, ½) the structure of the selenate was mapped on the most similar configuration of the LT-phase of alunogen. The calculations showed the following average atomic displacements (in Å) between the positions of corresponding atoms in the sulfate and the selenate: <Al–Al> = 0.184; <S–Se> = 0.190; oxygen atoms from slab-type A: <O–O> = 0.220; oxygen atoms from slab-type B: <O–O> = 0.709. In more detail, there is only one significant and very large shift of almost 2.438 Å between the position of Ow5 in LT-alunogen and the corresponding oxygen atom (O29) of the selenate in slab-type B pointing to differences in the local arrangement of the free water molecules. Notably, these positions are only partially occupied in both compounds. Nevertheless, the vast majority of the atoms can be superimposed onto each other within a few tenths of an Ångstrom. The measure of similarity Δ, as defined by Bergerhoff et al. (1999), has a value of 0.064.

Investigations concerning the phase transition

DSC measurements

DSC curves, confirming the reversible RT ↔ LT phase transformation, are given in Figure 5. The RT-form shows an exothermic phase transition to the LT-polymorph at a temperature

below –40° C on cooling. Upon heating, the endothermic back-transformation is observed above –10° C with a very low enthalpy of transformation of 0.3 ± 0.1 kJ mol^{-1}.

X-ray powder diffraction

The temperature-dependent sequence of powder diffraction patterns collected between 19.2 to 20.85° 2θ given in Figure 6 clearly shows that (i) the transformation can be followed by X-ray diffraction and (ii) that this 2θ region can be used to differentiate between the two polymorphs. Upon heating, the transformation starts at about -50 °C and is finished at about -30 °C. The pattern recorded at -40° C shows a co-existence of both phases. Although both modifications exhibit pronounced structural similarities (which will be discussed later) it is obvious that the transition is of first order.

Raman spectrosccopy

The Raman spectrum of the triclinic ambient temperature phase is in very good agreement with literature data (RRUFF Database of Mineral Properties, http://www.rruff.info/ima; Wang and Zhou 2014). Principally, four normal modes of vibrations have to be distinguished for the tetrahedral $[SO_4]$-groups (Myneni 2000). The so-called ν_1 and ν_2 modes represent the symmetric stretching and deformation vibrations, whereas the ν_3 and ν_4 modes conform to the corresponding asymmetric stretching and deformation vibrations. These vibrational modes occur in specific regions of the Raman spectrum which have been studied frequently (Myneni 2000 and references cited therein). According to these investigations the prominent observed bands for triclinic alunogen were allocated to the four abovementioned modes (see Table 4). The vibrational modes of the octahedral $Al(H_2O)_6$-moities contribute to the Raman spectrum as well. Their unambiguous assignment, however, is much more difficult. As was discussed by Boujelbene and Mhiri (2011) for a chemically related ammonium alum $(NH_4)Al(SO_4)_2 \cdot 12H_2O$, the relevant modes occur in regions of the anion bending modes,

librational modes of the H_2O molecules, and external modes. Due to the large number of symmetrically independent water molecules it is not surprising that in the characteristic region for the OH-stretching vibrations between 3000 and 3600 cm^{-1} only a broad unspecific hump could be observed, in agreement with the results of Wang and Zhou (2014).

However, the primary goal of this spectroscopic study was not to derive a complete allocation of all bands but to (i) verify if Raman spectroscopy is a suitable tool to differentiate between both forms and (ii) identify a spectral region which is especially suited for this purpose. As could be expected from the structural studies, the direct comparison between the Raman spectra of the ambient and the low-temperature modification shows striking similarities (see Figure 7). Nevertheless, there are small but significant differences in the region of the ν_2 vibrations which could be used for the discrimination between the two polymorphs (see Table 4).

Variable-temperature Raman spectroscopy combined with principal component analysis (PCA) allowed us to follow the thermally induced phase transformation between the RT- and LT- forms of alunogen. The sample was cooled/heated (temperature range 0 °C ↔ –100 °C) and Raman spectra were recorded every 10 °C. The measured Raman intensities in the spectral range 1200 to 95 cm^{-1} were then used as input variables for PCA. The objective of PCA is to describe the variation in data with a minimum of new, uncorrelated variables (principal components) (Martens and Naes 1989). The new variables (loadings) can be interpreted like spectra (Roggo et al. 2007). Groupings and trends, as well as outliers, can be detected with PCA (Gabrielsson et al. 2002). The multivariate data treatment method was applied to explain the variance-covariance structure of the 573 original variables (i.e. individual Raman intensities). The first principal component (t[1]) was constructed to extract the maximum variance in the data set. Further principal components extracted the maximum remaining variance which is uncorrelated with the variance of the previous principal components. By studying the loadings, which express how the old variables (Raman

intensities) are linearly combined, specific wavenumbers that influence the grouping of samples in the score plots (Figures 8 and 9) could be identified. Thus, PCA can reveal the variables, or combination of variables that determine some inherent structure in the data set (Wold et al. 2002; Jorgensen 2006).

Each two principal components (PCs: t[1] and t[2]) were needed to explain the data variance in the recorded Raman spectra following the phase transformations (RT → LT and LT → RT). The first principal components (t[1]), accounting for 52.5% of the data variability in Figure 8 and for 66.4% in Figure 9, separates the HT from the LT phase, as indicated by a step in the (regression) lines. The temperature effect on the Raman spectra is indicated by the slope of the (regression) lines. On cooling the phase transformation was observed at a temperature below –50 °C (Figure 8). The reverse transformation occurred at a temperature above –30 °C on heating (Figure 9). Again, a pronounced hysteresis is noticed.

Discussion and outlook

The crystal structures of both alunogen polymorphs are closely related. This is already indicated by the similarity between the monoclinic and the triclinic unit-cell metrics. As can be easily recognized from the comparison of Figures 10a and 10b the similarity is not restricted to the respective set of lattice parameters. In both modifications the same slab-types A and B are observed. Furthermore, the two forms exhibit a ...ABA'B'... stacking sequence along the *b*-axis. However, the AB and A'B' pairs are related by different symmetry operations: 2_1-screw axes (for the LT-form) and inversion centers (for the RT-phase). As was already noted by Menchetti and Sabelli (1974) the triclinic polymorph contains pseudo-mirror planes perpendicular to [010] and this feature was used to explain the characteristic twinning frequently observed in alunogen crystals. Actually, a closer inspection of the atomic coordinates of the LT-form revealed the same kind of pseudo-symmetry. This prompted us to look for a hypothetical aristotype or parent structure from which both phases can be derived. In order to simplify the investigations we restricted our considerations to the polyhedral parts

of both polymorphs ($Al(H_2O)_6$- and SO_4-units), i.e. the spatially more flexible "free" or "zeolitic" water molecules of the type B slabs were excluded. Obviously, the monoclinic space group $P2_1/m$ could be a good candidate for the symmetry of the potential aristotype. For the necessary analysis the program PSEUDO (Capillas et al. 2011) was employed. The software is able to find pseudo-symmetry in a crystal structure S with space group symmetry H when it can be derived from a virtual parent structure in a higher symmetry G using a left coset decomposition of G with respect to H: $G = H + g_2H + \ldots + g_nH$. In the next step the structure S to be tested is compared with the transformed structures g_iS. If the differences between the corresponding pairs of atoms in S and g_iS are below a certain threshold δ_{max}, the presence of a pseudo-symmetry is indicated. In case of alunogen, $G = P2_1/m$ is a minimal supergroup of $H_1 = P2_1$ and $H_2 = P\,\bar{1}$, respectively. Therefore, the test was applied twice for S_1 (LT-form) and S_2 (RT-form) and, indeed, for a maximum tolerance of 1.5 Å the *same* hypothetical aristotype in $G = P2_1/m$ could be derived for both cases, the crystal structure of which is presented in Figure 10c.

As a further group-theoretical concept to rationalize the distortions triggering the symmetry reduction from the hypothetical parent structure to the observed LT- and RT-forms, a symmetry mode analysis was performed using the program AMPLIMODES (Perez-Mato et al. 2010). In the course of this procedure the structural distortions present in a low-symmetry structure are decomposed into contributions from different modes, whose symmetries are given by the irreducible representations of the space group of the parent phase. The mode decomposition indicated that the resulting primary displacement fields can be allocated to order parameters transforming according the Γ_1^- (for LT-alunogen) and Γ_2^+ (for RT-alunogen) irreducible representations of $P2_1/m$. For the LT-phase, the resulting displacements for the most strongly affected sulfate tetrahedra have been visualized in Figure 11 using the program VESTA 3 (Momma and Izumi, 2011). It is obvious that the distortions are quite different not only what concerns the amplitudes but also what concerns the general type of the movements

of the atoms. With respect to their positions in the parent phase the tetrahedra of slab-type A are approximately shifted about 0.50 Å as a whole along the [100] direction (Figure 11a). The slab-type B tetrahedra in turn are rotated around one of the S-O bonds by an angle of about 50°. The corresponding displacements of the three oxygen atoms in the basal plane of the rotated polyhedra are about 1.50 Å (Figure 11b). In the triclinic RT-phase the same principal types of distortion can be observed. The main difference between the two modifications is due to different rotation senses of the tetrahedra in slab-type B. As can be seen from a comparison between in slabs B and B' in Figures 10a and 10b the basal planes of the tetrahedra about S3 in the LT-polymorph exhibit an opposite sense of rotation whereas the corresponding moieties in the RT-form rotate concordantly.

As a concluding remark, we would like to point out that alunogen is another example for a hydrous mineral whose temperature-dependent and dehydration behavior is only rudimentarily understood – at least from a structural point of view. In nature only the existence of meta-alunogen (Náray-Szabó 1969; Gordon 1942) with a probable water content of 13.5 H_2O molecules p.f.u. and monoclinic or orthorhombic symmetry has been reported. A crystallographic description of meta-alunogen is not available. Furthermore, the thermo-analytical studies mentioned in the introduction point to other intermediate hydrates before the water-free aluminum sulfate $Al_2(SO_4)_3$ is formed. This offers the perspective for more detailed *in-situ* studies and currently we are working on a comprehensive picture of how high-temperature and moisture influence the structural characteristics of alunogen.

Implications

Hydrous sulfates belong to the group of secondary minerals that have been observed to be ubiquitous on the Martian surface using both orbital remote sensing and data obtained from landed missions. Within this context, alunogen has attracted interest because it is one of the sulfates with the highest water content. Actually, alunogen as a hydrous aluminum sulfate has

443 been postulated to exist on Mars as a result of acid-sulfate weathering of basaltic materials
444 (Golden et al. 2005). Only recently, more detailed laboratory investigations showed that the
445 formation of alunogen in hydrothermal alteration studies of basaltic glasses strongly depends
446 if acid-vapor or acid-fluid experiments were performed (Hausrath et al. 2013). Therefore, the
447 detection of alunogen was suggested as a potential proxy for the fluid transport on Mars
448 implying reactions with either vapor or liquid water. In order to generate more reliable
449 physico-chemical information alunogen has been studied for the first time under Mars-
450 relevant temperature conditions using thermal, spectroscopic and diffraction techniques. Our
451 investigations show that alunogen undergoes a reversible structural phase transition upon
452 cooling. In particular, precise location of the hydrogen atoms has established the nature of the
453 complete complex hydrogen bonding scheme of the low-temperature modification. The new
454 data may help in the identification of this mineral by X-ray diffraction of Martian soils using
455 the Curiosity Rover's ChemMin instrument (Bish et al. 2014) or by Raman spectroscopy and,
456 therefore, may be used to connect these mission findings to more fundamental processes of
457 hydrological and geochemical importance that have occurred in the near-surface regions of
458 Mars. From a crystallographic point of view the phase transition in alunogen represents a text
459 book example for the rare case of a first-order phase transformation resulting in a single-
460 crystal-to-single-crystal transition.
461

462 **Acknowledgement**

463 The authors would like to thank Stuart Mills, Uwe Kolitsch, Diego Gatta (associate editor)
464 and an anonymous technical editor for their helpful comments and suggestions. DEB
465 acknowledges funding by the Hertha Firnberg Programme of the Austrian Science Fund
466 (FWF, project T593-N19). We are grateful to Dr. Kurt Schenk (EPF Lausanne, Switzerland)
467 for running exploratory DSC experiments.

468 **References**

Agilent (2012) CrysAlis PRO. Agilent Technologies, Yarnton, Oxfordshire, England.

Audra, P., and Hobléa, F. (2007) The first cave occurence of jurbanite [Al(OH SO_4)·$5H_2O$, associated with alunogen [$Al_2(SO_4)_3$·$17H_2O$] and tschermigite [$NH_4Al(SO_4)_2$·$12H_2O$]: thermal-sulfidic serpents cave, France. Journal of Cave and Karst Studies, 69, 243-249.

Bai, G., Xu, P., Li, P., and Wand, T. (2011) Thermal decomposition kinetic mechanism of aluminium sulfate hydrates. Advanced Materials Research, 177, 238-244.

Barret, P., and Thiard R. (1965) Étude des degrés d'hydratation du sulfate d'aluminium par microthermogravimétrie et microanalyse thermique différentielle associées sous pression de vapeur d'eau constante. Comptes rendus hebdomadaires des séances de l'Académie des Sciences, 260, 2823-2826.

Bayliss, P. (1964) Some properties of alunogen from New South Wales. American Mineralogist, 49, 1763-1766.

Bell, M.S. (2014) Experimental alteration of basalt to support interpretation of remote sensing and *in situ* measurements from Mars. 45th Lunar and Planetary Science Conference, PDF-No. 2822.

Bergerhoff, G., Berndt, M., Brandenburg, K., and Degen, T. (1999) Concerning inorganic crystal structure types. Acta Crystallographica B, 55, 147-156.

Bibring, J.-P., Langevin, Y., Mustard, J.F., Poulet, F., Arvidson, R., Gendrin, A., Gondet, B., Mangold, N., Pinet, P., and Forget, F. (2006) Global mineralogical and aqueous Mars history derived from OMEGA/Mars express data. Science, 312, 400-404.

Bish, D.L., Blake, D.F., Vaniman, D.T., Chipera, S.J., Morris, R.V., Ming, D.W., Treiman, A.H., Sarrazin, P., Morrison, S.M., Downs, R.T., Achilles, C.N., Yen, A.S., Bristow, T.F., Crisp, J.A., Morookian, J.M., Farmer, J.D., Rampe, E.B., Stolper, E.M., Spanovich, N., and the MSL Science Team (2013) X-ray Diffraction Results from

Mars Science Laboratory: Mineralogy of Rocknest at Gale Crater. Science, 341, 1238932-1-5.

Bish, D., Blake, D., Vaniman, D., Sarrazin, P., Bristow, T., Achilles, C., Dera, P., Chipera, S., Crisp, J., Downs, R.T., Farmer, J., Gailhanou, M., Ming, D., Morookian, J. M., Morris, R., Morrison, S., Rampe, E., Treiman, A., and Yen, A. (2014) The first X-ray diffraction measurements on Mars. IUCrJ, 1, 514-522.

Boudon, G., Villemant, B., Komorowski, J.C., Ildefonse, P., Hammouya, P., and Semet, M. (1996) The hydrothermal system of the Soufriere Hills volcano, Montserrat (West Indies): chemical, mineralogical and microtextural signatures in fluids, altered rocks and 1995-96 tephra. MVO/VSG-Open Scientific Meeting, Volcano Study Group. The Geological Society, Burlington House, London.

Boujelbene, M., and Mhiri, T. (2011) Polarized Raman Spectra of $NH_4Al(SO_4)_2 \cdot 12H_2O$. International Journal of Spectroscopy, Article ID 128601, 6 pages.

Brese, N.E., and O'Keeffe, M. (1991) Bond-valence parameters for solids. Acta Crystallographica B, 47, 192-197.

Brown I.D., and Altermatt, D. (1985) Bond-valence parameters obtained from a systematic analysis of the Inorganic Crystal Structure Database. Acta Crystallographica B, 41, 244-247.

Burla, M.C., Caliandro, R., Camalli, M., Carrozzini, B., Cascarano, G.L., DeCaro, L., Giacovazzo, G., Polidori, G., and Spagna, R. (2005) SIR2004: an improved tool for crystal structure determination and refinement. Journal of Applied Crystallography, 38, 381-388.

Capillas, C., Tasci, E.S., de la Flor, G., Orobengoa, D., Perez-Mato, J.M., and Aroyo, M.I. (2011) A new computer tool at the Bilbao Crystallographic Server to detect and characterize pseudosymmetry. Zeitschrift für Kristallographie, 226, 186-196.

Chou, K.-S., and Soong, C.-S. (1984) Kinetics of the multistage dehydration of

aluminium sulphate hydrate. Thermochimica Acta, 81, 305-310.

Çilgi, G.K., and Cetişli, H. (2009) Thermal decomposition kinetics of aluminum sulfate hydrate. Journal of Thermal Analysis and Calorimetry, 98, 855-861.

Clark, R.C. and Reid, J.S. (1995) The analytical calculation of absorption in multifaceted crystals. Acta Crystallographica A, 51, 887-897.

Coelho, A. (2007) TOPAS Academic Version 4.1. Computer Software, Topas Academic, Coelho Software, Brisbane.

Dowty, E. (2011) ATOMS, Version 6.4, Shape Software, Kingsport, USA.

Fang, J.H., and Robinson, P.D. (1976) Alunogen, $Al_2(H_2O)_{12}(SO_4)_3 \cdot 5H_2O$: its atomic arrangement and water content. American Mineralogist, 61, 311-317.

Farrugia, L.J. (2012) WinGX and ORTEP for Windows: an update. Journal of Applied Crystallography, 45, 849-854.

Flack, H.D. (1983) On enantiomorph-polarity estimation. Acta Crystallographica A, 39, 876-881.

Földvári, M. (2011) Handbook of thermogravimetric system of minerals and its use in geological practice, 213, 1-180. Occasional Papers of the Geological Institute of Hungary, Budapest, Hungary.

Gabrielsson, J., Lindberg, N. O., and Lundstedt, T. (2002) Multivariate methods in pharmaceutical applications. Journal of Chemometrics, 16, 141-160.

Golden, D.C., Ming, D.W., Morris, R.V., and Mertzman, S.A. (2005) Laboratory-simulated acid-sulfate weathering of basaltic materials: implications for formation of sulphates at Meridiani Planum and Gusev crater, Mars. Journal of Geophysical Research, 110, E12S07, 1-15.

Gordon, S.G. (1942) Results of the Chilean mineralogical expedition of 1938. Part VII.- The crystallography of alunogen, meta-alunogen, and pickeringite. Notulae Naturae of the

Academy of Natural Sciences of Philadelphia, 101, 1-9.

Haberle, R.M. (2013) Estimating the power of Mars' greenhouse effect. Icarus, 223, 619–620.

Hausrath, E.M., Golden, D.C., Morris, R.V., Agresti, D.G., and Ming, D.W. (2013) Acid sulfate alteration of fluoroapatite, basaltic glass and olivine by hydrothermal vapors and fluids: implications for fumarolic activity and secondary phosphate phases in sulfate-rich Paso Robles soil at Gusev Crater, Mars. Journal of Geophysical Research: Planets, 118, 1-13.

Hawthorne, F.C., Krivovichev, S.V., and Burns, P.C. (2000) The crystal chemistry of sulphate minerals. In C.N. Alpers, J.L. Jambor, and D.K. Nordstrom, Eds. Sulfate Minerals – Crystallography, Geochemistry, and Environmental Significance, 40, 1-112. Reviews in Mineralogy and Geochemistry, Mineralogical Society of America, Chantilly, Virginia.

Herri, J.-M., and Chassefière, E. (2012) Carbon dioxide, argon, nitrogen and methane clathrate hydrates: Thermodynamic modeling, investigation of their stability in martian atmospheric conditions and variability of methane trapping. Planetary and Space Science, 73, 376–386.

Jambor , J.L., Nordstrom, D.K., and Alpers, C.N. (2000) Metal sulphate salts from sulphide mineral oxidation. In C.N. Alpers, J.L. Jambor, and D.K. Nordstrom, Eds. Sulfate Minerals – Crystallography, Geochemistry, and Environmental Significance, 40, 303-350. Reviews in Mineralogy and Geochemistry, Mineralogical Society of America, Chantilly, Virginia.

Jorgensen, A.C., Miroshnyk, I., Karjalainen, M., Jouppila, K., Siiria, S., Antikainen, O., and Rantanen, J. (2006) Multivariate data analysis as a fast tool in evaluation of solid state phenomena. Journal of Pharmaceutical Sciences, 95, 906-916.

Kounaves, S.P., Hecht, M.H., Kapit, J., Quinn, R.C., Catling, D.C., Clark, B.C., Ming,

D.W., Gospodinova, K., Hredzak, P., McElhoney. K., and Shusterman, J. (2010) Soluble sulphate in the martian soil at the Phoenix landing site. Geophysical Research Letters, 37, L09201, 1-5.

Krivovichev, S.V. (2006) Crystal chemistry of selenates with mineral-like structures. I. $(Al(H_2O)_6)_2\ (SeO_4)_3(H_2O)_4$ - the selenate analogue of alunogen. Zapiski Vserossijskogo Mineralogicheskogo Obshchestva, 135, 106-113. (in Russian).

Kruszewski, Ł. (2013) Supergene sulphate minerals form the burning coal mining dumps in the Upper Silesian Coal Basin, South Poland. International Journal of Coal Geology, 105, 91-109.

Larsen, E.S., and Steiger, G. (1928) Dehydration and optical study of alunogen, nontronite, and griffithite. American Journal of Science, 15, 1-19.

Martens, H. and Naes, T. (1989) Multivariate Calibration. John Wiley & Sons, Chichester, 419pp.

Martin, R., Rodgers, K.A., and Browne, P.R.L. (1999) The nature and significance of sulphate-rich aluminous efflorescences from the Te Kopia geothermal field, Taupo Volcanic Zone, New Zealand. Mineralogical Magazine, 63, 413-419.

Menchetti, S. and Sabelli, C. (1974) Alunogen: Its structure and twinning. Tschermaks Mineralogische und Petrographische Mitteilungen, 21, 164-178.

Mills, S.J., Nestola, F., Kahlenberg, V., Christy, A.G., Hejny, C., and Redhammer, G.J. (2013) Looking for jarosite on Mars: The low-temperature crystal structure of jarosite. American Mineralogist, 98, 1966-1971.

Momma, K. and Izumi, F. (2011) *VESTA 3* for three-dimensional visualization of crystal, volumetric and morphology data. Journal of Applied Crystallography, 44, 1272-1276.

Myneni, S.C.B. (2000) X-ray and vibrational spectroscopy of sulfate in Earth materials. In C.N. Alpers, J.L. Jambor, and D.K. Nordstrom, Eds. Sulfate Minerals – Crystallography, Geochemistry, and Environmental Significance, 40, 113-172.

598 Reviews in Mineralogy and Geochemistry, Mineralogical Society of America,
599 Chantilly, Virginia.
600 Náray-Szabó, I. (1969) Über die Hydrate des Aluminiumsulfats. Acta Chimica
601 Academiae Scientiarum Hungaricae, 60, 27-36.
602 Palache, C., Berman, H., and Frondel, C. (1951) The System of Mineralogy of James Dwight
603 Dana and Edward Salisbury Dana, Yale University 1837-1892, Volume II. John Wiley
604 and Sons, Inc., New York, 7th edition, revised and enlarged, 537-540.
605 Perez-Mato, J.M., Orobengoa, D., and Aroyo, M.I. (2010) Mode crystallography of
606 distorted structures. Acta Crystallographica A, 66, 558-590.
607 Prince, E. (Ed.) (2004) International Tables for Crystallography, Volume C.
608 Mathematical, Physical and Chemical Tables. 3rd Edition. Kluwer Academic
609 Publishers, Dordrecht/ Boston/ London. 1000 pp.
610 Robinson, K., Gibbs, G.V., and Ribbe, P.H. (1971) Quadratic elongation: a
611 quantitative measure of distortion in coordination polyhedra. Science, 172, 567-570.
612 Roggo, Y., Chalus, P., Maurer, L., Lema-Martinez, C., Edmond, A., and Jent, N. (2007) A
613 review of near infrared spectroscopy and chemometrics in pharmaceutical
614 technologies. Journal of Pharmaceutical and Biomedical Analysis, 44, 683-700
615 Sheldrick, G.M. (2008) A short history of *SHELX*. Acta Crystallographica A, 64, 112-122.
616 Spek, A.L. (2009) Structure validation in chemical crystallography. Acta
617 Crystallographica D, 65, 148-155.
618 Stracher, G.L., Prakash, A., Schroeder, P., McCormack, J., Zhang, X., van Dijk, P.,
619 and Blake, D. (2005) New mineral occurrences and mineralization processes: Wuda
620 coal-fire gas vents of Inner Mongolia. American Mineralogist, 90, 1729-1739.
621 Swayze, G.A., Ehlmann, B.L., Milliken, R.E., Poulet, F., Wray, J.J., Rye, R.O., Clark, R.
622 N., Desborough, G.A., Crowley, J.K., Gondet, B., Mustard, J.F., Seelos, K.D.,
623 Murchie, S.L. (2008) Discovery of the Acid-Sulfate Mineral Alunite in Terra Sirenum,

Mars, Using MRO CRISM: Possible Evidence for Acid-Saline Lacustrine Deposits? EoS Transactions of the American Geophysical Union, Fall Meeting Supplement , 89, Abstract P44A-04.

Tasci, E.S., de la Flor, G., Orobengoa, D., Capillas, C., Perez-Mato, J.M., and Aroyo, M.I. (2012) An introduction to the tools hosted in the Bilbao Crystallographic Server. EPJ Web of Conferences, 22, 00009, 1-22.

Umetrics (2005) Simca-P Version 11.0, Umetrics AB, Umea, Sweden.

Wang, A., and Zhou, Y. (2014) Experimental comparison of the pathways and rates of the dehydration of Al-, Fe-, Mg- and Ca-sulfates under Mars relevant conditions. Icarus, 234, 162-173.

Wold, S., Berglund, A., and Kettanen, N. (2002) New and old trends in chemometrics. How to deal with the increasing data volumes in research, development and production – with examples from pharmaceutical research and process modeling. Journal of Chemometrics, 16, 377-386.

Figure captions

Figure 1. Rietveld plot of the X-ray powder diffraction pattern of the monoclinic LT-form of alunogen collected at -100 °C. Observed step intensities are represented by a black line. Calculated step intensities (in red) have been modeled based on the crystal structure obtained from the single-crystal diffraction study. Tick marks for the Bragg peaks are given. The lower blue line represents the difference curve between observed and calculated step intensities.

Figure 2. Coordination polyhedra around (a) Al1 and (b) Al2 shown with displacement ellipsoids drawn at the 60% probability level.

Figure 3. Projection of a single slab of type A parallel to *c**. Blue spheres correspond to oxygen atoms. Hydrogen atoms are shown as small black spheres. Alternating chains of (unconnected) octahedra and tetrahedra can be identified.

Figure 4. View of a single slab of type B perpendicular to (010). Dark blue spheres correspond to oxygen atoms. The light blue spheres represent the partially occupied water site Ow5. Hydrogen atoms are shown as small black spheres. Hydrogen bonds within the slab are given as thin dashed lines.

Figure 5. DSC thermograms of synthetic alunogen, recorded at heating/cooling rates of 10 °C min^{-1}.

Figure 6. Sequence of powder diffraction patterns acquired for temperatures from -100 °C to 20 °C in steps of ΔT = 10 °C. The selected range between 19.2 and 20.8 °2θ can be used to follow the phase transition between the monoclinic LT- and the triclinic RT- modification. At -40 °C both phases coexist.

Figure 7. FT Raman spectra of the alunogen polymorphs: red – high-temperature form (recorded at 0 °C), blue – low-temperature form (recorded at –60 °C). Insert shows the spectral range 1200 to 95 cm^{-1} enlarged.

Figure 8. Raman principal component analysis (PCA) score plot for the first principal component (t[1]) of the alunogen phases occurring during cooling from 0 to –100 °C. Each triangle corresponds to a Raman spectrum recorded at different temperatures. 52.5% of the data variance was modelled by t[1].

Figure 9. Raman principal component analysis (PCA) score plot for the first principal component (t[1]) of the alunogen phases occurring during heating from –100 to 0 °C. Each triangle corresponds to a Raman spectrum recorded at different temperatures. 66.4% of the data variance was modelled by t[1].

Figure 10. Comparison between the crystal structures of the (a) monoclinic LT- and (b) triclinic RT-form of alunogen in projections parallel to *c**. Crystallographic data of the latter polymorph have been taken from the paper of Menchetti & Sabelli (1974). However, for sake clarity the origin has been shifted by (½,0,0). (c) Hypothetical aristotype of both polymorphs in space group $P2_1/m$.

Figure 11. Distortions of the sulfate tetrahedra with respect to their positions in the parent phase. (a) Tetrahedra of slab-type A are approximately shifted about 0.50 Å as a whole along the [100] direction. (b) Slab-type B tetrahedra in turn are rotated around one of the S-O bonds by an angle of about 50°. The corresponding displacements of the three oxygen atoms in the basal plane of the rotated polyhedra are about 1.50 Å.

687 Table 1. Crystal data and structure refinement parameters for the LT-polymorph of alunogen.

Empirical formula	$Al_2(SO_4)_3 \cdot 16.61H_2O$
Formula weight	641.39
Wavelength	0.71073 Å
Temperature	-100(2) °C
Crystal system	monoclinic
Space group	$P2_1$
Unit cell dimensions	a = 7.4125(3) Å
	b = 26.8337(16) Å
	c = 6.0775(3) Å
	β = 97.312(4)°
Volume	V = 1199.01(10) $Å^3$
Z	2
Density (calculated)	1.780 Mg/m^3
Absorption coefficient	0.501 mm^{-1}
F(000)	672
Crystal size	0.44 x 0.13 x 0.01 mm^3
Theta range for data collection	2.87 to 26.02°
Exposure time per frame	60 s
Scan type	ω-scans (0.5 °)
Crystal-to-detector distance	70 mm
Index ranges	-9<=h<=8, -30<=k<=33, -5<=l<=7
Reflections collected	6594
Independent reflections	3887 [R(int) = 0.0363]
Completeness to theta 26.02	99.0%
Max. and min. transmission	0.9950 and 0.8095
Refinement method	Full-matrix least-squares on F^2
Data / restraints / parameters	3887 / 52 / 411
Goodness-of-fit on F^2	1.047
Final R indices [I>2σ(I)]	R1 = 0.0377, wR2 = 0.0817
R indices (all data)	R1 = 0.0443, wR2 = 0.0861
Largest diff. peak and hole	0.48 and -0.37 e.$Å^{-3}$

688

689

Table 2. Atomic coordinates and equivalent isotropic displacement parameters (Å^2) for the LT-polymorph of alunogen. All atoms occupy general positions. U_{eq} is defined as one third of the trace of the orthogonalized U_{ij} tensor. Isotropic displacement parameters of the H-atoms of the water molecules were coupled to those of the corresponding oxygen atoms according to $U_{iso}(H) = 1.2 \times U_{eq}(O)$. The water position Ow5 is only partially occupied (61(1)%). Bond valence sums (BVS) in *v.u.* for the non-hydrogen atoms have been calculated including O–H and H…O contributions.

	x	*y*	*z*	U_{eq}/U_{iso}	BVS
S1	0.7898(1)	0.5619(1)	0.5178(1)	0.013(1)	5.95
S2	0.7348(1)	0.9393(1)	0.5132(1)	0.011(1)	5.91
S3	0.3566(2)	0.7523(1)	0.5220(2)	0.026(1)	6.02
Al1	0.2954(2)	0.5989(1)	0.0033(2)	0.012(1)	2.98
Al2	0.2466(1)	0.9011(1)	0.9959(2)	0.011(1)	2.99
O1	0.9452(3)	0.5905(1)	0.4561(4)	0.019(1)	2.04
O2	0.8513(3)	0.5339(1)	0.7242(4)	0.022(1)	1.96
O3	0.6405(3)	0.5957(1)	0.5545(4)	0.022(1)	2.03
O4	0.7247(3)	0.5265(1)	0.3372(5)	0.022(1)	2.00
O5	0.6692(3)	0.9750(1)	0.3356(5)	0.019(1)	2.00
O6	0.5857(3)	0.9050(1)	0.5487(4)	0.017(1)	2.00
O7	0.7990(3)	0. 9662(1)	0.7212(4)	0.018(1)	1.97
O8	0.8901(3)	0.9107(1)	0.4454(4)	0.014(1)	2.14
O9	0.5271(5)	0.7517(2)	0.4220(5)	0.053(1)	2.01
O10	0.2183(4)	0.7820(1)	0.3868(5)	0.034(1)	1.99
O11	0.3918(4)	0.7731(1)	0.7488(5)	0.029(1)	1.97
O12	0.2892(5)	0.7007(1)	0.5333(5)	0.036(1)	2.04
O13	0.0656(3)	0.5767(1)	0.0654(4)	0.018(1)	1.96
O14	0.3447(3)	0.6250(1)	0.2900(4)	0.017(1)	2.00
O15	0.1955(4)	0.6589(1)	-.1048(5)	0.021(1)	1.98
O16	0.2495(3)	0.5710(1)	-.2810(4)	0.013(1)	1.98
O17	0.3988(3)	0.5375(1)	0.1095(4)	0.014(1)	1.95
O18	0.5314(3)	0.6178(1)	-.0525(5)	0.016(1)	1.98
O19	0.1644(3)	0.8408(1)	0.8748(4)	0.016(1)	2.07
O20	0.2038(3)	0.9307(1)	0.7125(4)	0.013(1)	1.99
O21	0.0093(3)	0.9191(1)	1.0465(5)	0.017(1)	1.99
O22	0.3375(3)	0.9623(1)	1.1138(4)	0.015(1)	2.01

729	O23	0.4860(3)	0.8853(1)	0.9468(4)	0.016(1)	1.96
730	O24	0.2880(3)	0.8733(1)	1.2822(4)	0.015(1)	2.02
731	Ow1	0.7048(4)	0.8254(1)	0.2100(5)	0.026(1)	1.73
732	Ow2	0.6121(4)	0.7111(1)	0.0392(5)	0.030(1)	2.04
733	Ow3	0.8405(5)	0.8061(2)	0.7919(7)	0.050(1)	1.77
734	Ow4	-.0040(5)	0.7107(2)	0.1215(6)	0.051(1)	1.94
735	Ow5	0.8523(8)	0.7073(3)	0.6096(10)	0.053(2)	1.60
736	H131	-.0270(40)	0.5636(14)	-.0130(50)	0.021	
737	H132	0.0270(40)	0.5845(14)	0.1860(40)	0.021	
738	H141	0.4380(30)	0.6143(12)	0.3700(60)	0.020	
739	H142	0.3220(40)	0.6532(9)	0.3440(60)	0.020	
740	H151	0.1300(40)	0.6818(11)	-.0470(50)	0.025	
741	H152	0.2380(50)	0.6765(12)	-.2030(50)	0.025	
742	H161	0.1520(30)	0.5755(13)	-.3720(50)	0.016	
743	H162	0.2860(40)	0.5424(9)	-.3170(60)	0.016	
744	H171	0.5020(30)	0.5325(13)	0.1900(60)	0.017	
745	H172	0.3370(40)	0.5117(10)	0.1220(60)	0.017	
746	H181	0.5660(50)	0.6474(7)	-.0380(60)	0.019	
747	H182	0.5750(50)	0.6048(12)	-.1590(50)	0.019	
748	H191	0.2390(30)	0.8192(11)	0.8580(70)	0.019	
749	H192	0.0580(20)	0.8321(13)	0.8420(60)	0.019	
750	H201	0.2210(50)	0.9609(7)	0.6920(60)	0.016	
751	H202	0.1070(30)	0.9225(12)	0.6320(60)	0.016	
752	H211	-.0670(40)	0.9301(14)	0.9450(40)	0.020	
753	H212	-.0390(40)	0.9143(15)	1.1610(40)	0.020	
754	H221	0.4490(20)	0.9667(14)	1.1530(60)	0.018	
755	H222	0.2780(40)	0.9804(12)	1.1850(60)	0.018	
756	H231	0.5570(40)	0.8643(12)	1.0230(50)	0.019	
757	H232	0.5310(40)	0.8887(14)	0.8260(40)	0.019	
758	H241	0.3840(30)	0.8818(12)	1.3570(60)	0.018	
759	H242	0.2640(40)	0.8441(8)	1.3030(60)	0.018	
760	Hw11	0.7760(40)	0.8409(13)	0.3100(50)	0.031	
761	Hw12	0.6450(40)	0.8060(13)	0.2900(50)	0.031	
762	Hw21	0.5520(50)	0.7330(12)	-.0490(50)	0.036	
763	Hw22	0.5760(50)	0.7211(15)	0.1630(40)	0.036	
764	Hw31	0.7740(60)	0.7845(15)	0.8480(70)	0.060	
765	Hw32	0.8420(70)	0.7960(19)	0.6600(40)	0.060	
766	Hw41	0.0110(60)	0.7389(10)	0.1750(80)	0.061	
767	Hw42	-.1150(30)	0.7064(17)	0.0730(90)	0.061	

Hw51	0.7400(30)	0.7080(40)	0.5490(100)	0.063	
Hw52	0.9100(70)	0.7030(40)	0.4950(160)	0.063	

Table 3. Selected individual and average bond lengths [Å], bond angles [°], polyhedral volumes [$Å^3$] and distortion parameters (QE: quadration elongation; AV: angle variance) for the LT-polymorph of alunogen.

S1-O3	1.470(3)	S1-O1	1.472(3)	
S1-O2	1.483(3)	S1-O4	1.484(3)	
<S1-O>	1.477	Volume	1.654	
QE	1.000	AV	0.494	
S2-O6	1.475(3)	S2-O5	1.477(3)	
S2-O7	1.481(3)	S2-O8	1.485(3)	
<S2-O>	1.480	Volume	1.662	
QE	1.000	AV	0.629	
S3-O10	1.465(3)	S3-O9	1.470(3)	
S3-O12	1.477(3)	S3-O11	1.479(3)	
<S3-O>	1.473	Volume	1.640	
QE	1.000	AV	0.576	
Al1-O15	1.855(3)	Al1-O14	1.869(3)	
Al1-O16	1.875(3)	Al1-O13	1.888(3)	
Al1-O18	1.893(3)	Al1-O17	1.897(3)	
<Al1-O>	1.880	Volume	8.845	
QE	1.001	AV	1.784	
Al2-O19	1.849(3)	Al2-O22	1.881(3)	
Al2-O24	1.881(3)	Al2-O23	1.885(3)	
Al2-O21	1.886(3)	Al2-O20	1.887(3)	
<Al2-O>	1.878	Volume	8.831	
QE	1.000	AV	1.175	
O3-S1-O1	110.18(17)		O3-S1-O2	109.92(16)
O1-S1-O2	108.27(14)		O3-S1-O4	109.06(15)
O1-S1-O4	109.63(16)		O2-S1-O4	109.76(17)
O6-S2-O5	109.11(15)		O6-S2-O7	110.17(16)
O5-S2-O7	110.35(16)		O6-S2-O8	109.84(16)
O5-S2-O8	109.07(16)		O7-S2-O8	108.28(15)

O10-S3-O9	110.6(2)	O10-S3-O12	108.63(19)	
O9-S3-O12	108.8(2)	O10-S3-O11	110.20(17)	
O9-S3-O11	109.3(2)	O12-S3-O11	109.33(17)	
O15-Al1-O14	91.62(14)	O15-Al1-O16	90.19(13)	
O14-Al1-O16	178.18(14)	O15-Al1-O13	90.91(13)	
O14-Al1-O13	90.36(12)	O16-Al1-O13	89.71(12)	
O15-Al1-O18	92.37(13)	O14-Al1-O18	89.52(13)	
O16-Al1-O18	90.30(12)	O13-Al1-O18	176.73(14)	
O15-Al1-O17	179.11(14)	O14-Al1-O17	89.12(13)	
O16-Al1-O17	89.06(12)	O13-Al1-O17	89.57(12)	
O18-Al1-O17	87.16(12)			
O19-Al2-O22	177.96(14)	O19-Al2-O24	91.62(13)	
O22-Al2-O24	89.15(13)	O19-Al2-O23	90.55(13)	
O22-Al2-O23	87.56(13)	O24-Al2-O23	90.65(13)	
O19-Al2-O21	91.29(13)	O22-Al2-O21	90.60(13)	
O24-Al2-O21	89.81(13)	O23-Al2-O21	178.10(15)	
O19-Al2-O20	89.81(13)	O22-Al2-O20	89.45(13)	
O24-Al2-O20	178.37(15)	O23-Al2-O20	90.13(12)	
O21-Al2-O20	89.37(12)			

Table 4. Comparison between the Raman bands (cm^{-1}) of the sulfate groups in the monoclinic and the triclinic polymorphs of alunogen.

Vibrational modes	Monoclinic form (–60 °C)	Triclinic form (0 °C)
ν_2	438 (shoulder), 455, 470	465
ν_4	612, 642 (shoulder)	612
ν_1	992	992
ν_3	1074, 1089, 1127	1067 (shoulder), 1086, 1126

Figure 1

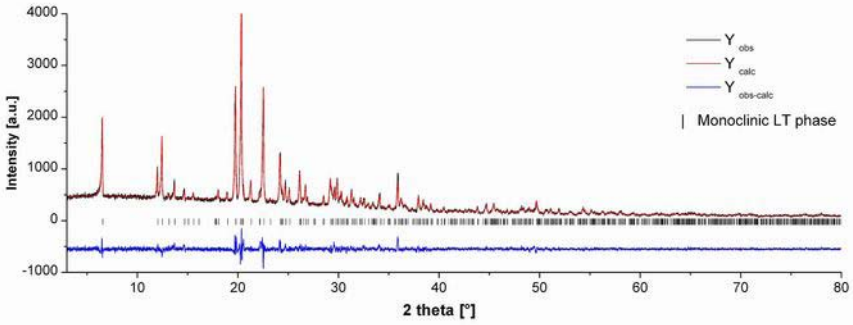
4000
3000
2000
1000
0
-1000
Intensity [a.u.]
10
20
30
40
50
60
70
80
2 theta [°]
Y obs
Y calc
Y obs-calc
Monoclinic LT phase

Figure 2a

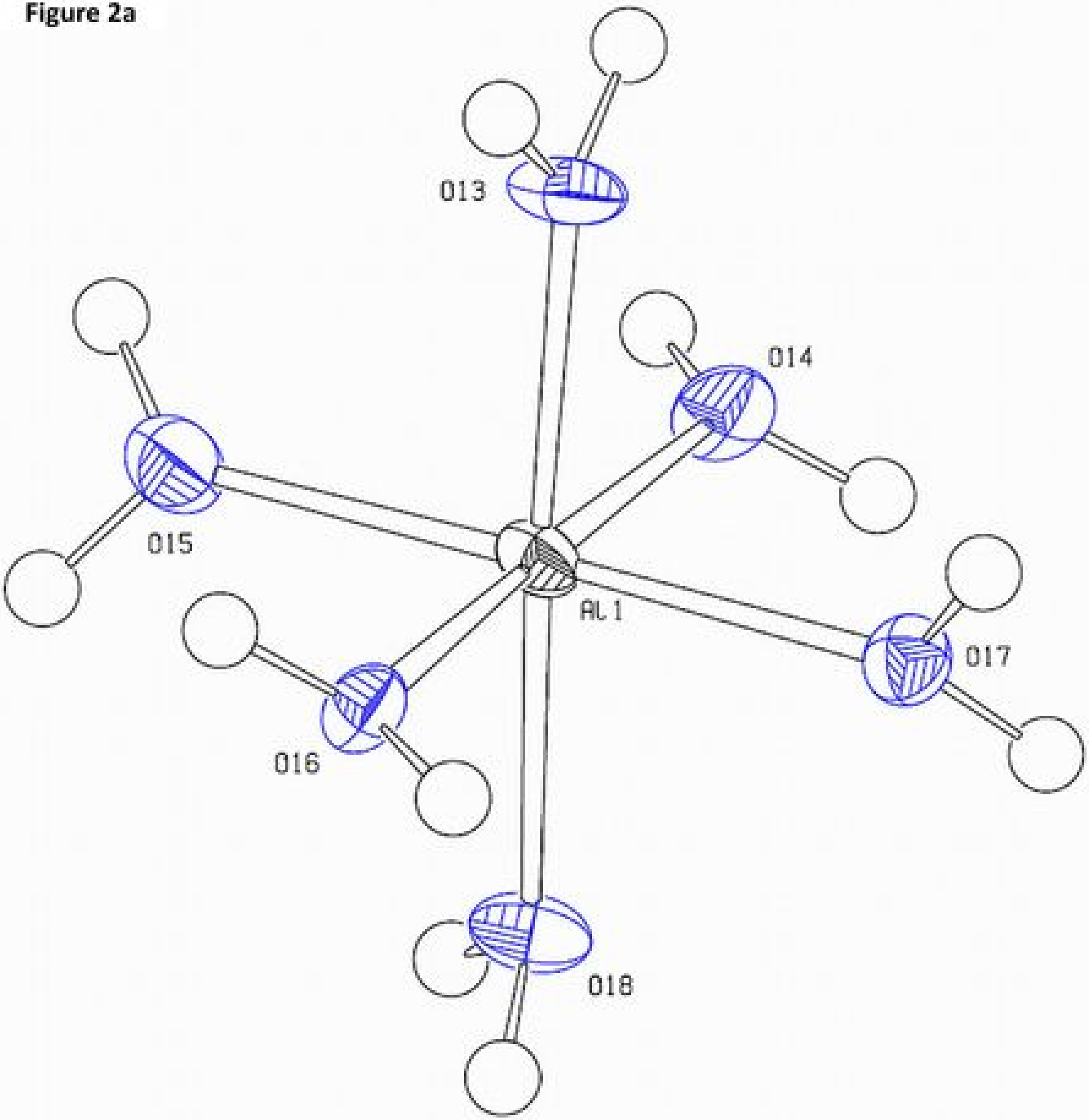

Figure 2b

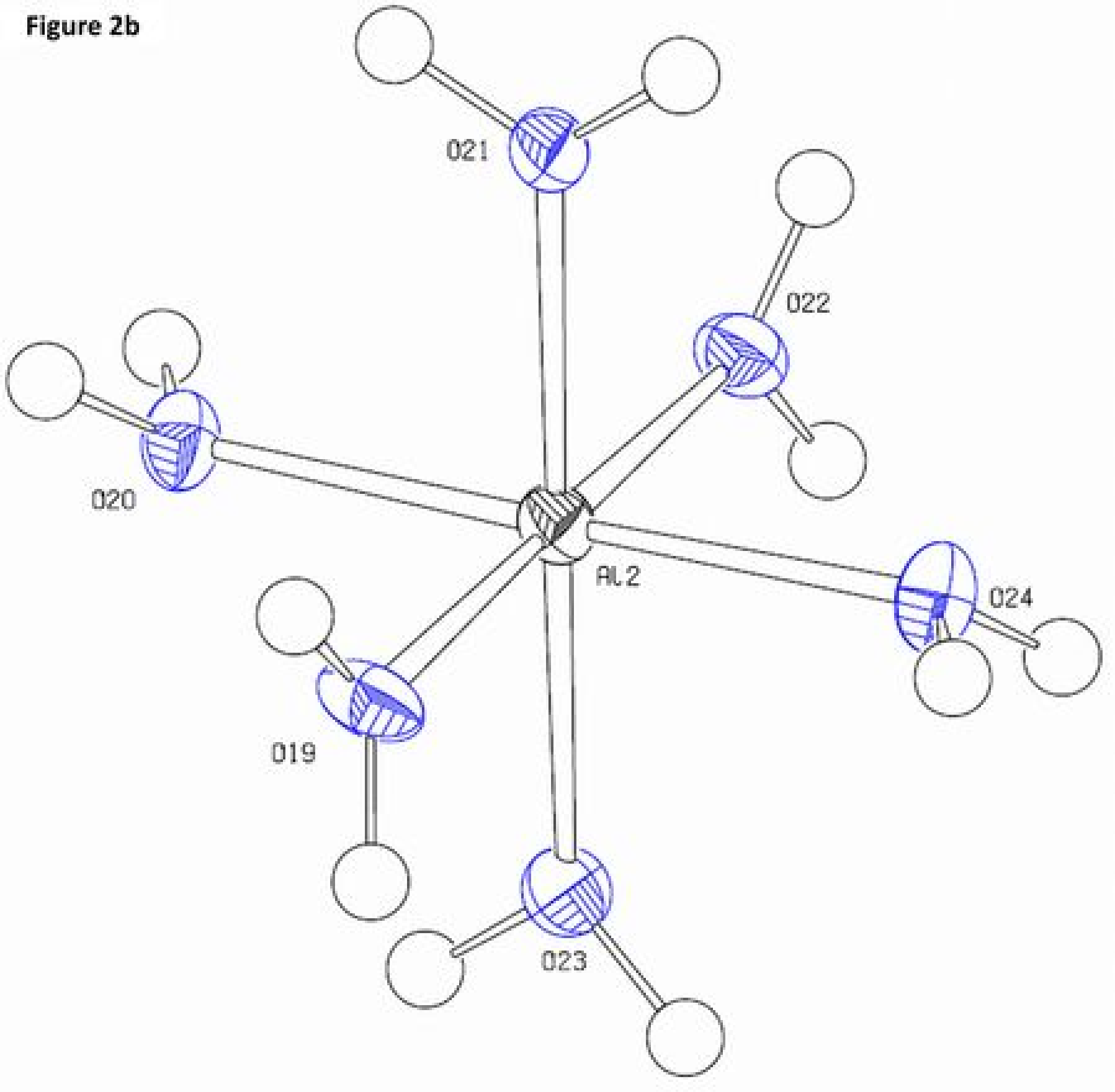

Figure 3

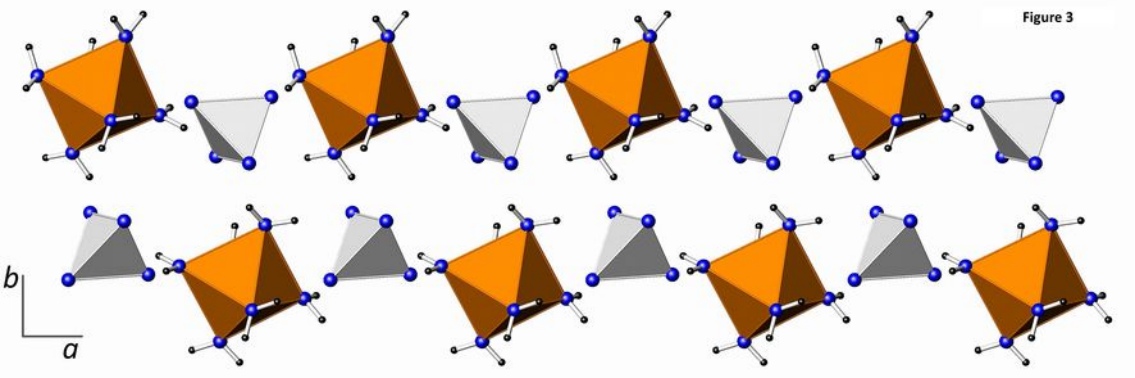

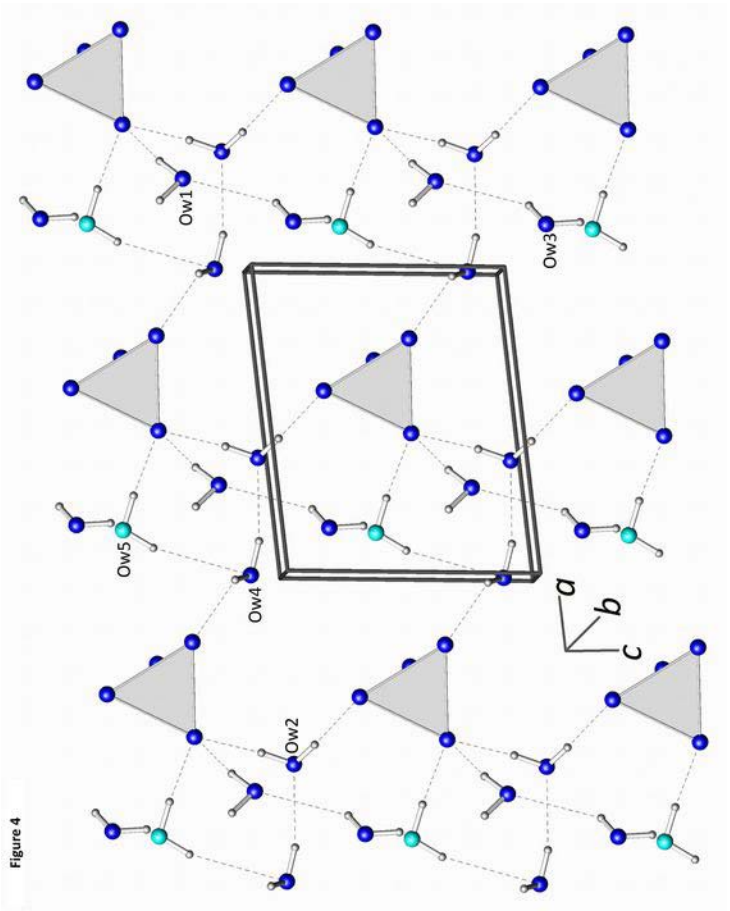

Figure 4

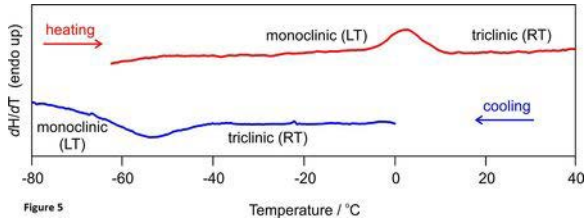
heating
monoclinic (LT)
triclinic (RT)
cooling
monoclinic
(LT)
triclinic (RT)
dH/dT (endo up)
-80
-60
-40
-20
0
20
40
Temperature / °C

Figure 5

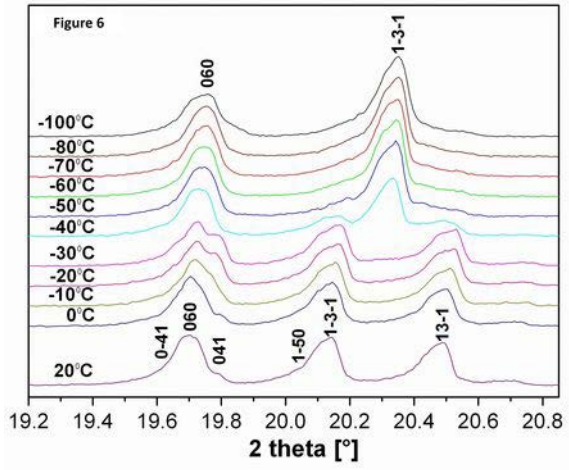
Figure 6
060
1-3-1
-100°C
-80°C
-70°C
-60°C
-50°C
-40°C
-30°C
-20°C
-10°C
0°C
20°C
0-41
060
041
1-50
1-3-1
13-1
19.2
19.4
19.6
19.8
20.0
20.2
20.4
20.6
20.8
2 theta [°]

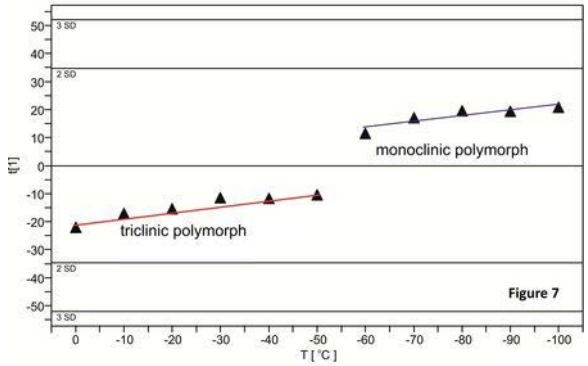
3 SD
2 SD
2 SD
3 SD
monoclinic polymorph
triclinic polymorph
t[1]
T [°C]
50
40
30
20
10
0
-10
-20
-30
-40
-50
0
-10
-20
-30
-40
-50
-60
-70
-80
-90
-100

Figure 7

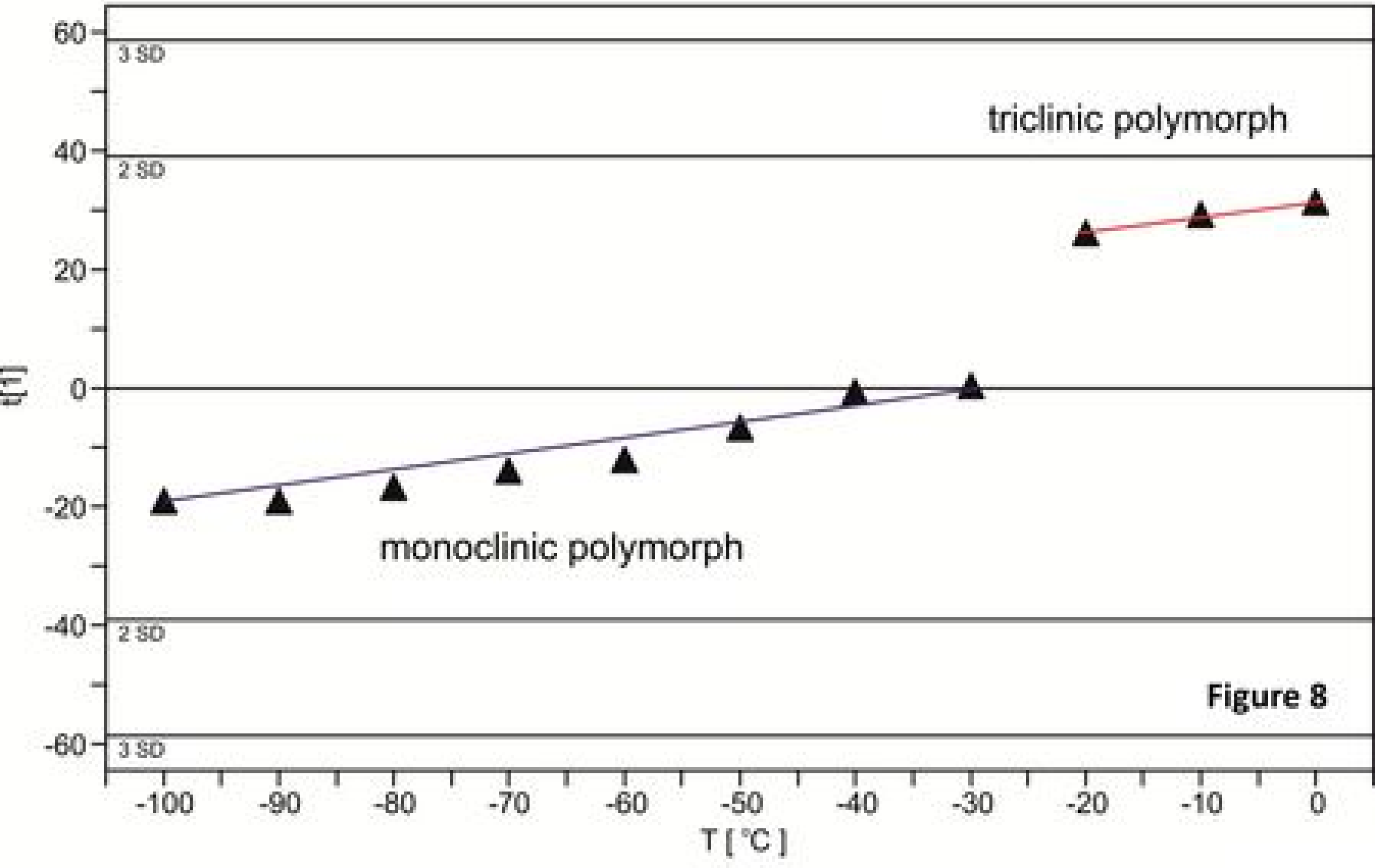
60
3 SD
40
2 SD
20
0
-20
-40
2 SD
-60
3 SD
triclinic polymorph
monoclinic polymorph
-100
-90
-80
-70
-60
-50
-40
-30
-20
-10
0
T [°C]

Figure 8

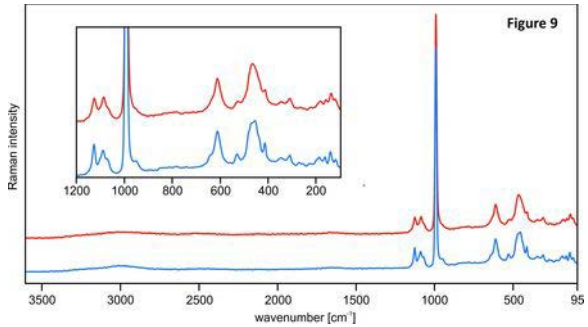
Figure 9
Raman intensity
1200
1000
800
600
400
200
3500
3000
2500
2000
1500
1000
500
95
wavenumber [cm⁻¹]

Figure 10a

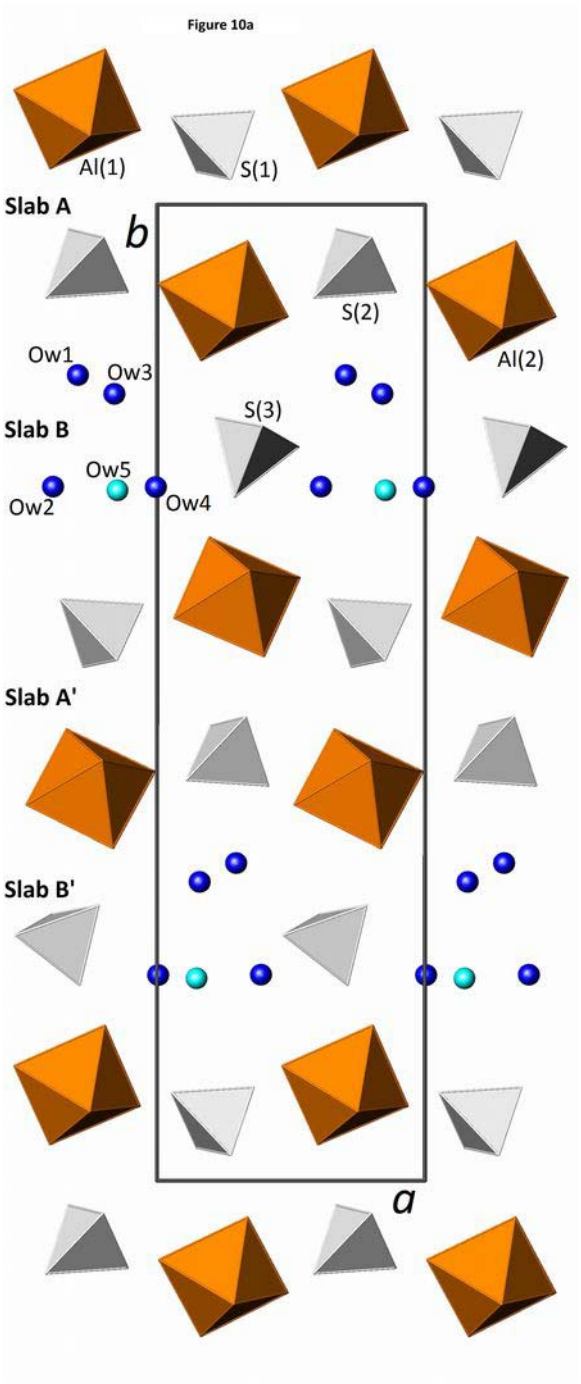

Figure 10b

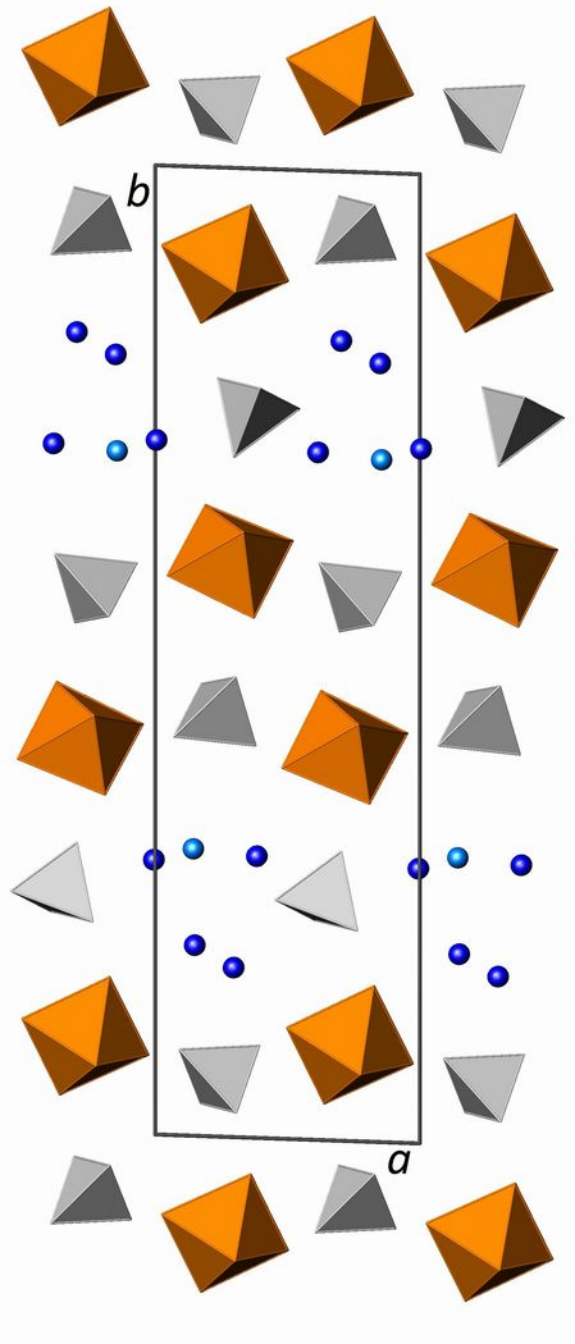

Figure 10c

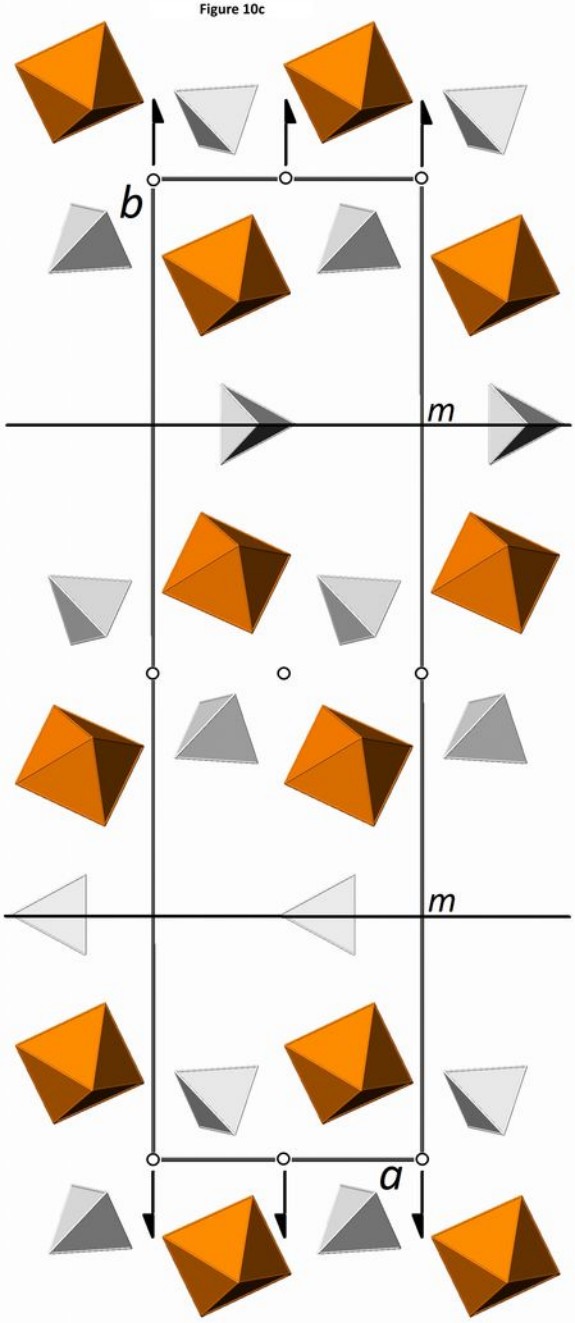

Figure 11a

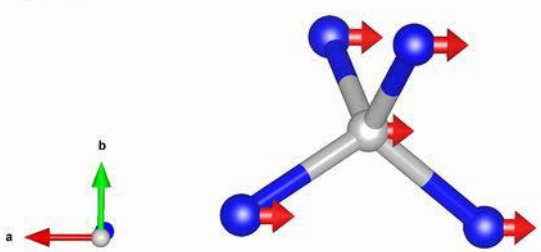

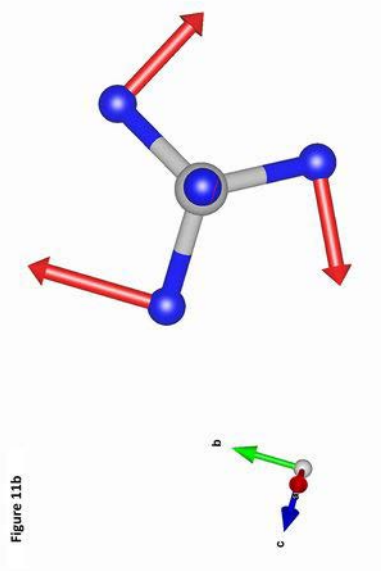

Figure 11b